POLARIMETRIC SCATTERING ANALYSIS IN FULLY POLARIMETRIC SAR

PI No.025

Hiroyoshi Yamada[1], *Yoshio Yamaguchi*[1]

[1]Department of Information Engineering, Niigata University,
Ikarashi 2-8050, Nishi-Ku, Niigata 950-2181, Japan
E-mail: yamada@ie.niigata-u.ac.jp

1. INTRODUCTION

Land surface classification is one of the important applications of POLSAR (Polarimetric SAR) image analysis. Since the POLSAR images have multi-polarization images of HH, HV, VH, and HH polarization, the scattering nature of terrain can be effectively discriminated. There are many classification techniques such as simple HV basis imaging, the Pauli basis imaging, H-Alpha-Anisotropy imaging [1], power decomposition imaging [2]-[7]. The most frequently used method is the H-Alpha-Anisotropy based on the eigenvalues of coherency matrix. The second one is the scattering power decomposition based on physical scattering models, which was first developed by A. Freeman and S. Durden [2]. The extended methods were proposed by our group with additional components, the helix component and several types of volume scattering components [3],[4].

As for the scattering power decomposition techniques the covariance matrix or coherency matrix obtained by POLSAR images is used for the decomposition. In these types of techniques, we have many unknowns to be determined such as power of each component and some of the elements in each component-covariance matrices. The number of unknowns exceeds to the number of independent observables in POLSAR images. Therefore some assumptions are adopted to obtain unique solution. For example, in the Freeman decomposition, they adopted two assumptions. The first assumption is that the volume scattering components is known, which can be modeled by return from cloud of randomly oriented dipoles. The second is that the (1,1)- elements in the covariance matrix for single or double-bounce component is known (plus or minus one) [2]. In the Yamaguchi's decomposition, they added several additional volume scattering matrices. In this technique, we should select suitable one among the candidates of volume scattering covariance matrices that can be estimated by the co-polarization power ratio [3]. Accuracy of decomposition in these techniques depends on the validity of the assumptions. When some of the assumptions cannot holds good, negative power components often appear.

Recently, Dr. Arii, et. al., proposed modified volume scattering model for the power decomposition [5]-[7]. They used the model for POLSAR data set and an adaptive technique with a model-error term is employed to overcome the negative-power problem [6].

In this research, we first focus on the model-based scattering mechanism decomposition problem, especially to verify the modified volume scattering model proposed by Dr. Arii and van Zyl. Then, availability of the polarization rotation proposed by our group [8] to the model is also verified. The polarization rotation is the basis transform to minimize cross-polarization terms in the covariance matrix, which enables us to decrease volume scattering component and increase double bounce in the oriented urban, where oriented means that the buildings are not aligned parallel to the orbit. These verifications are done with the ALOS/PALSAR data of Sapporo, Japan. The modified model can estimate roughness and orientation of the distributed trunks and branches in the forest. By using this feature, we also propose a new index to discriminate forest and vegetation areas from urban area.

We have been also considering the extended model-based decomposition for POL-InSAR dataset [9]-[14]. Although reliable results for ALOS/PALSAR data could not be obtained at this stage due to temporal decorrelation of repeat pass observation, concept of the approach will be available for the future study. Hence, summary of these techniques are also included before conclusions.

2. OVERVIEW OF VARIOUS MODEL-BASED DECOMPOSITION TECHNIQUES

2.1. Freeman-Durden model [2]

The Freeman-Durden model is the most famous model based decomposition model by using physical or canonical scattering models such as single, double-bounce, and volume scattering components. By using these models, covariance matrix of the POLSAR data can be decomposed by

$$\boldsymbol{C} = f_s \boldsymbol{C}_s + f_d \boldsymbol{C}_d + f_v \boldsymbol{C}_v , \qquad (1)$$

where C_s, C_d, and C_v are the covariance matrices of the single, double and volume scattering component, respectively, as shown in Fig.1. The single-bounce component is dominant in the open surface such as bare-soil and sea surface, and the double-bounce component is dominant in the urban-area especially for the buildings which locates along the azimuth track. The volume component is dominant in the forest and vegetation area. Therefore, to determine the coefficients in (1), f_s, f_d, and f_v, and estimate each component ratio becomes very powerful tool for the POLSAR data analysis.

(a) Single-bounce (b) Double-bounce (c) Volume
Fig.1. Typical Scattering Mechanizm

When reflection symmetry holds, we only have 4 independent observables in C. Therefore, they proposed to determine C_v as derived by the random oriented dipole clouds to shown the volume scattering components in the forest canopy, and assume that one of the component in C_s or C_d is known to make the problem solvable. This decomposition is effective to many POLSAR data. However there is a problem of negative power component. For the area where volume scattering component is dominant, single or double-bounce component becomes negative. This is caused by the assumption denoted above.

2.2. Yamaguchi model [3],[4]

To alleviate the problem, Yamaguchi *et. al.*, have extend the model in (1) as

$$C = f_s C_s + f_d C_d + f_v C_v + f_h C_h . \qquad (2)$$

where C_h is the helix component. In addition, they introduce three types of C_v s depending on their dipole distribution. Selection of suitable C_v at given patch can be done by using co-pol power ratio. The number of patches that have negative power component becomes smaller than the Freeman model. The helix component is not dominant in almost all the areas with enough number of multilooks. Therefore, extension of the volume scattering model can be considered to alleviate the problem. However, there still remain patches having negative power component. To resolve this inconvenience, they roll up small power components to the others.

2.3. Arii-van Zyl model [5]

Recently, Dr.Arii and van Zyl have proposed a new decomposition method by using modified volume scattering model. In their model, the covariance matrix is decomposed as

$$C = f_s C_s + f_d C_d + f_v C_v(\sigma,\theta) + C_r , \qquad (3)$$

where σ and θ corresponds to the roughness and orientation of the dipole cloud distribution, respectively. This volume scattering model can be said as the generalized model of Yamaguchi's volume scattering component. They also introduce the new component, C_r, for the residue.

This kind of extension always makes problem solvable. However, they successfully make the problem solvable as the minimization problem of residue among unknown variables [6]. The computer burden of this decomposition is heavy compared to the previous ones, nevertheless this decomposition is very attractive. Main cause of the negative power component is model error of each component. All the model errors can be included in the residue component. Therefore no negative power component occurs in this decomposition. Furthermore, we can obtain additional information of roughness and orientation in the forest area. In the followings, we call this volume scattering model as "modified volume scattering model".

3. VERIFICATION OF THE MODIFIED VOLUME SCATTERING MODEL

3.1. Experimental data

In the verification of the volume scattering model, ALOS data of Sapporo, Japan was employed. Detailed data specification and its optical image are listed below. As can be seen in Fig.1, urban and vegetation area are located at the right-middle, left-middle in this image. The rightmost and leftmost areas are the forest. The blue area is the Sea.

Table.1 Experimental data set

Area	Sapporo and environs
Observed data	July 29, 2009
Polarization	HH, HV, VH, VV
Sensor	ALOS/PALSAR (L-band)
Incident angle	21.5 degree
Multilooks	3 x 18 (Azimuth x Range)

Fig.2 Optical image of the test site (Sapporo, Japan).

3.2. Derivation of f_v with the modified volume scattering model

Dr.Arii *et. al.*, developed Adaptive Non-Negative Eigenvalue Decomposition (ANNED) method [6], which is modified version of the Non-Negative Eigenvalue Decomposition (NNED) [15], to solve (3). In the first stage of the ANNED, we evaluate eigenvalue of the following matrix with given σ and θ by changing f_v,

$$\boldsymbol{C}' = \boldsymbol{C} - f_v \boldsymbol{C}_v(\sigma,\theta). \quad (3)$$

The best fit f_v can be determined which minimize power of the remainder $Tr[\boldsymbol{C}_v]$ in the condition of

$$Tr[\boldsymbol{C}_r] \geq 0, Tr[\boldsymbol{C}'] \geq 0, Tr[\boldsymbol{C}_v] \geq 0. \quad (4)$$

where $Tr[]$ denotes trace of a matrix. In their approach denoted in [5], one-dimensional search on f_v is required in addition to two dimensional search on σ and θ. It is time consuming.

In our research, we directly derive f_v by using generalized eigenvalue of

$$\left|\boldsymbol{C} - \lambda \boldsymbol{C}_v(\sigma,\theta)\right| = 0. \quad (5)$$

Since $\boldsymbol{C}$ is the 3x3 matrix, we have three eigenvalues, $\lambda_1 \geq \lambda_2 \geq \lambda_3$. If the volume scattering is correctly removed, rank of $\boldsymbol{C}'$ becomes 2 including single and double-bounce whose covariance matrixes have rank of 2. Therefore, it is clear that the best-fit f_v can be directly solved by

$$f_v = \lambda_3, \quad (6)$$

Except for the case that $\boldsymbol{C}_r(\sigma,\theta)$ becomes singular. This property was numerically checked. There was no significant difference between experimental results of (3) and (5). In the followings, we adopted the approach in (5).

3.3. Comparison of the decomposed results

The decomposed results of the Sapporo data by using Freeman-Druden and Arii-van Zly decomposition are shown in Fig3 and 4. Ps, Pd, and Pv denote power of the single, double-bounce and volume scatterings, respectively. In the false color images we allocate red, green and blue to Ps, Pv and Pd. As reported in several articles, Freeman method tends to overestimate power of volume scatterings. This tendency can be clearly seen in these figures. Contribution of the power of the single and double bounce in urban area becomes dominant in comparison with the power of the volume scatterings. In the urban area, we still see the relative strong volume scatterings. They become strong especially in the urban area where buildings/streets are not aligned parallel to the azimuth track of the SAR platform. This problem will be considered in the next section.

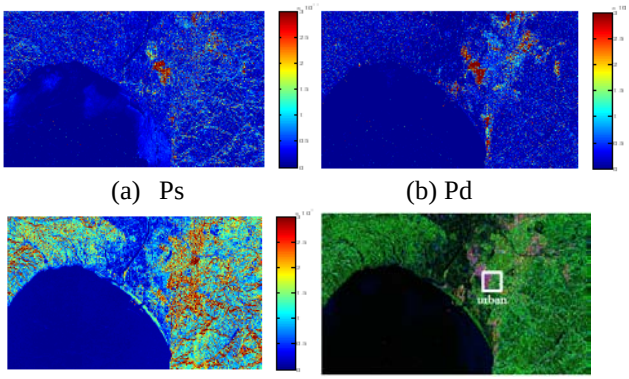

(a) Ps (b) Pd

(c) Pv (d) False color image

Fig.3 Decomposed results by using Freeman-Durden decomposition.

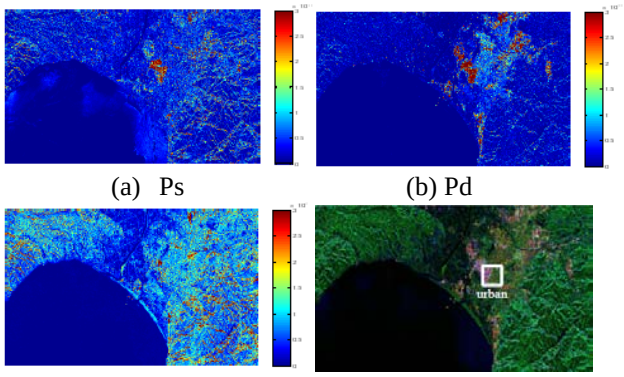

(a) Ps (b) Pd

(c) Pv (d) False color image

Fig.4 Decomposed results by using Arii-van Zyl decomposition.

3.4. Further analysis: Error Criterion

As denoted in (4), criterion in this minimization problem is

$$\text{Criterion I}: \min\left(Tr[\boldsymbol{C}_r]\right) \text{with } Tr[\boldsymbol{C}_r] \geq 0. \quad (7)$$

However, in the model matching sense, we can also adopt the following criterion.

$$\text{Criterion II}: \min\left(\sqrt{\|\boldsymbol{C}_r\|_F^2}\right) \text{with } Tr[\boldsymbol{C}_r] \geq 0 \quad (8)$$

where $\|\cdot\|_F$ denotes Frobenius norm. In the false color images we could not see the differences with both criteria. Difference can be seen in the estimated σ and θ as shown in Figs.5 and 6. Also, Trace and Frobenius norm of the derived remainders with Criterion I and II are shown in Figs. 7 and 8, respectively.

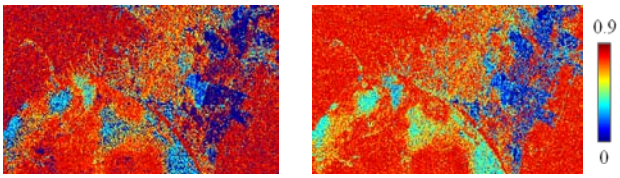

(a) Criterion I (b) Criterion II

Fig.5 Estimated roughness (σ)

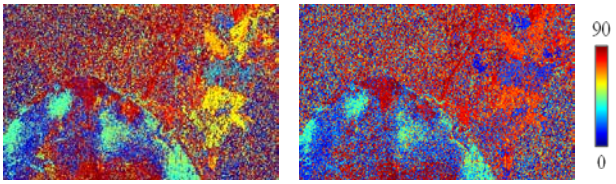

(a) Criterion I (b) Criterion II

Fig.6 Estimated orientation (θ)

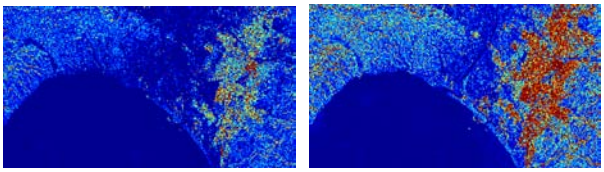

(a) Trace of $\boldsymbol{C}_r$ (b) Frobenius norm of $\boldsymbol{C}_r$

Fig.7 Remainder $\boldsymbol{C}_r$ with Criterion I.

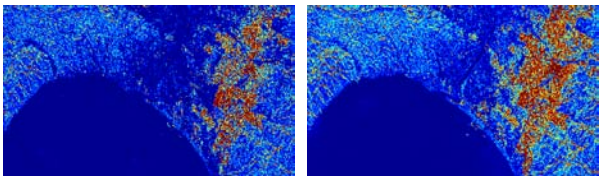

(a) Trace of $\boldsymbol{C}_r$ (b) Frobenius norm of $\boldsymbol{C}_r$

Fig.8 Remainder $\boldsymbol{C}_r$ with Criterion II.

The Criterion I adopted in [5] minimizes trace of $\boldsymbol{C}_r$, hence trace with Criterion I (Fig.7(a)) is smaller than that with Criterion II (Fig.7(b)). However, difference can be seen only in the urban area. This difference brings us the difference of σ and θ as shown in the Figs.5 and 6. However, when we see the forest and vegetation area, estimated σ and θ, and also remainders, are almost same in both criteria.

It is clear that the estimated results coincide with each other if the employed models are correctly matched to the observed scattering signals. The demonstrated results in this subsection are one of the evidence that the modified volume scattering model in (3) is valid for forest/vegetation analysis.

4. ORIENTED URBAN PROBLEM IN THE DECOMPOSITION

4.1 Polarimetric decomposition in urban area

The volume scattering model in (3) is intended to model tree branches and trunk distribution in forest. As discussed in the previous section, forest region can be well analyzed by the Arii's model. However, strong volume scattering remains in the urban area. Example of the false color images are shown in Fig.9. These are the close up images of urban area denoted white box in Figs.3(d) and 4(d).

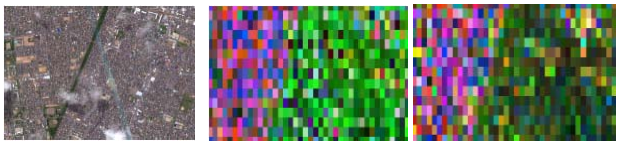

(a) (b) (c)

Fig.9 Optical and False color images in the urban area.
(a) optical image, (b) Freeman decomposition, (c) Arii decomposition

Intuitively, urban area has strong double bounce component when the buildings are aligned long the azimuth track of platform orbit. As shown in these figures, red and blue are dominant in the urban area which aligned parallel to the orbit ("pararel-urban"). However, green becomes dominant where the buildings are not aligned to the orbit ("oriented-urban") in both decompositions. Improvement can be seen in (c) , however there still remain dominant green patches.

4.2 Rotation of the polarization basis

To decrease the oriented urban effect in the decomposition, our group has proposed polarization basis transform to the original fully polarimetric data. The transformed scattering matrix is defined by

$$\boldsymbol{S}(\theta)=\begin{bmatrix}\cos\phi & \sin\phi\\ -\sin\phi & \cos\phi\end{bmatrix}\begin{bmatrix}S_{HH} & S_{HV}\\ S_{VH} & S_{VV}\end{bmatrix}\begin{bmatrix}\cos\phi & -\sin\phi\\ \sin\phi & \cos\phi\end{bmatrix}. \quad (9)$$

To minimize cross-polarized term, we can obtain the following expression for the rotation angle [8]

$$\tan 4\phi=\frac{4\,\mathrm{Re}\left\langle S_{HV}^{*}(S_{HH}-S_{VV})\right\rangle}{\left\langle\left|S_{HH}-S_{VV}\right|^{2}-4\left|S_{HV}\right|^{2}\right\rangle}. \quad (10)$$

Above transformation is derived in order to minimize closs-polarized term. However, transformation itself is an Unitary transform. Therefore, component power of the volume scattering must be unchanged if the model is correct.

4.3 Experimental results with the rotation

The experimental results with rotation are shown in Fig.10. Estimated area is the same as shown in Fig.4. Also false color images without and with rotation are shown in Fig.11. In this dataset, no big improvement can be seen. However, as can be seen in these figures, polarization basis rotation can be successfully applied to enhance double-bounce in the urban-area, especially to the oriented urban area, without loss of volume scattering power in the forest area. This is the important point to realize stable and robust decomposition. In the previous models in (1) and (2), power of the volume scattering often decreased and power of angle and double bounce were increased due to the imperfection of the volume scattering model. This problem seems to be resolved by the modified volume scattering model.

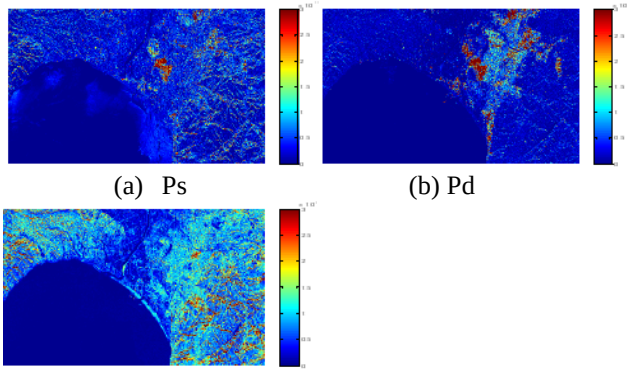

(a) Ps (b) Pd

(c) Pv

Fig.10 Decomposed results with rotation by using Arii-van Zyl decomposition.

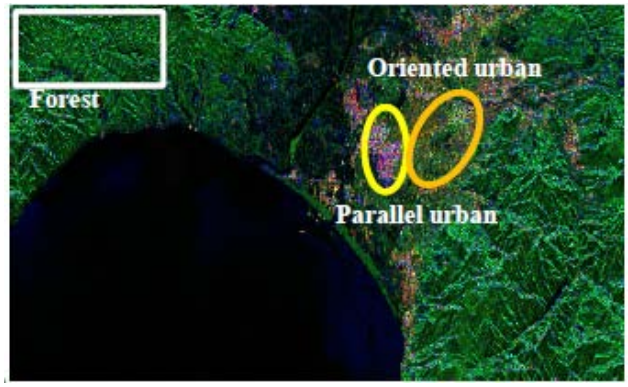

(a) without rotation

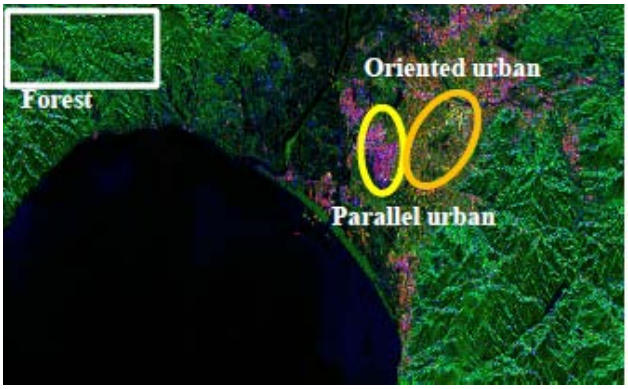

(b) with rotation

Fig.11 False color images with and without rotation.

5. APPLICATION OF THE MODIFIED VOLUE SCATTERING MODEL

5.1 Estimated roughness and orientation with rotation

One may want to see what happens in estimated roughness and orientation with rotation. The estimated σ and θ (Criterion I) with rotation are shown in Fig.12. For estimated orientation θ, large shift can be seen in the urban area but random phase shift can be also seen in the forest area (See Figs.12(a) and 6(a)). On the other hand, typical variation can be seen in the estimated roughness σ. In comparison with Figs. 12(b) and 5(a), roughness of the forest in almost unchanged by the rotation, however clear difference can be seen in the urban area including the oriented urban.

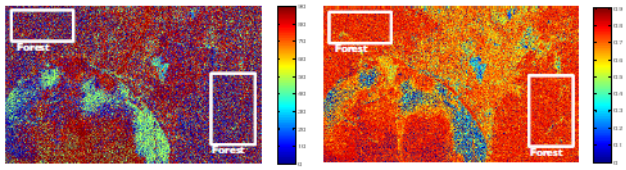

(a) orientation (b) roughness

Fig. 12 Estimated orientation and roughness with rotation

5.2 RVI for Forest/vegetation and urban area discrimination

Radar vegetation index (RVI) is one of the famous index to discriminate forest and vegetation area in the POLSAR images which is given by [17]

$$RVI = \frac{4\lambda_3}{\lambda_1 + \lambda_2 + \lambda_3} \tag{11}$$

where λ_3 is the smallest eigenvalue of $\boldsymbol{C}$. The RVI is adopted for the comparison in this section with light modification so as to limit its maximum to 1:

$$\Lambda = \frac{4\lambda_3}{\lambda_1 + \lambda_2 + \lambda_3} \tag{12}$$

The estimated result is shown in Fig.13.

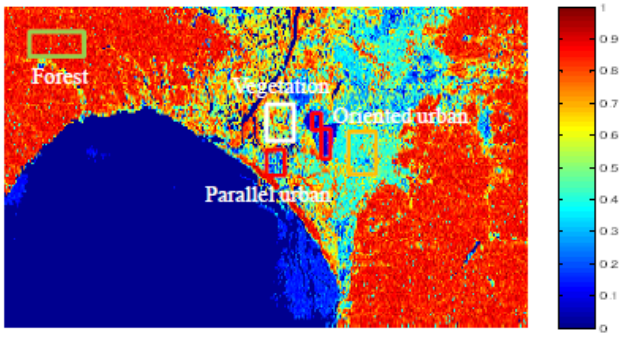

Fig.13 Radar vegetation index distribution

5.3 Roughness with rotation for Forest/vegetation and urban area discrimination

As denotes in Sect.5.1, roughness of the forest area seems to be almost stable. Figure 14 shows variation of roughness of the selected area in Fig.13 with rotation. Clearly, forest region is very stable, and vegetation (crop-field) and urban area show their own charactersitics.

When we employ the characteristic that the variation of σ with forest region is small, we can derive following index.

$$\sigma_1 = 1 - \frac{\Delta\sigma}{\sigma_0} \tag{13}$$

where $\Delta\sigma = \sigma_{\max}(\phi) - \sigma_{\min}(\phi)$ is defined by using maximum and minimum value of σ. σ_0 is 0.9069 which is upper limit of σ. By using this index, stable region such as forest shows high index.

In addition, the forest region shows the highest σ in comparison with those of other areas. Forest discrimination can be enhanced by using the following index.

$$\sigma_2 = \frac{\sigma_{\max}(\phi)}{\sigma_0}\left(1 - \frac{\Delta\sigma}{\sigma_0}\right) \qquad (14)$$

The estimated results by using index in (13) and (14) are shown in Fig.15.

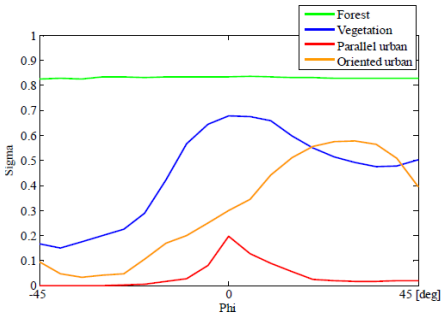

Fig.14 Variation of roughness with rotation in each area

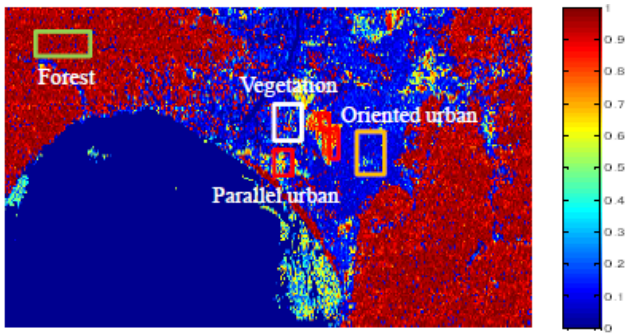

(a) Estimated results by using (13)

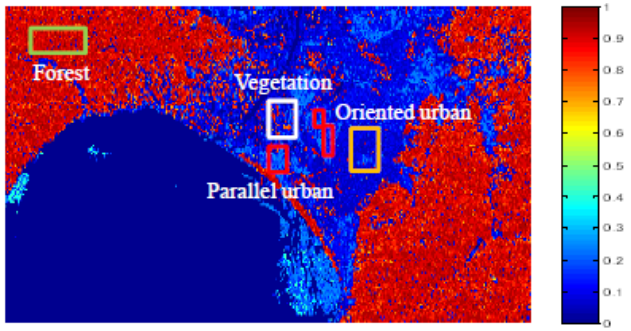

(b) Estimated results by using (14)

Fig.15 Forest discrimination by using roughness parameter with rotation

Histograms of the selected typical regions in each figure are shown in Figs.16(a), (b) and (c), respectively. The RVI index shows difference of characteristics for each typical area clearly, however the value sometimes overlaps in other area. If one wants to extract only the forest region, the index in (14) becomes a powerful tool.

Next, we'd like to consider the discrimination of urban area from vegetation and forest. Even we employ RVI, RVIs in vegetation and oriented-urban often have the same value as shown in Fig.16(a). When overlap of the curves for "vegetation" and "oriented-urban" becomes small we can improve discrimination performance. Several combinations of parameters were checked, and we found that the mean value of roughness with rotation is the potential index which is defined by

$$\bar{\sigma} = average(\sigma(\phi)) . \qquad (15)$$

Estimated results and their histograms are shown in Fig.17 and Fig.16(d), respectively. Improvement of discrimination performance between parallel/oriented-urban and vegetation (crop field)/forest can be realized as shown in Figs16(a) and (d).

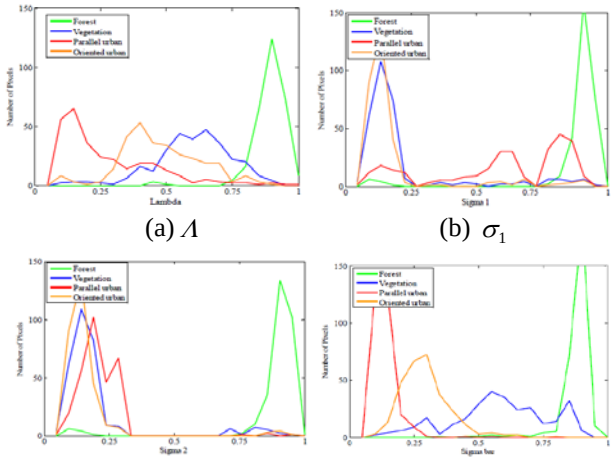

(a) Λ (b) σ_1

(c) σ_2 (d) $\bar{\sigma}$

Fig.16 Histograms of each index for various areas

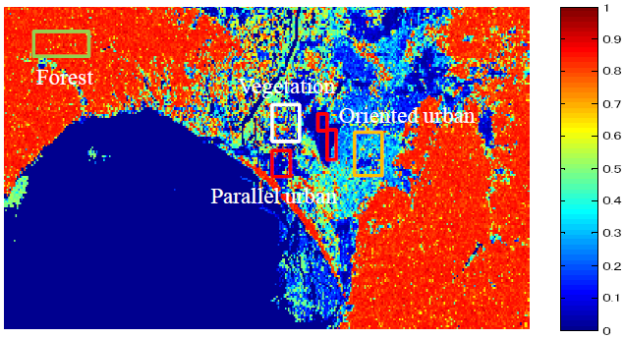

Fig.17 Vegetation/Forest/Urban discrimination by using roughness parameter with rotation by using (15)

Seasonal change detection is also the important to verify availability of index. Figures 18 and 19 show the estimated indexes and histogram of the selected areas for the winter season data. The data were taken at December

14, 2009. Since Sapporo is the snowy city, there were no crops in this season, and the fields were covered by snow. This tendency can be clearly seen in these results for both indexes.

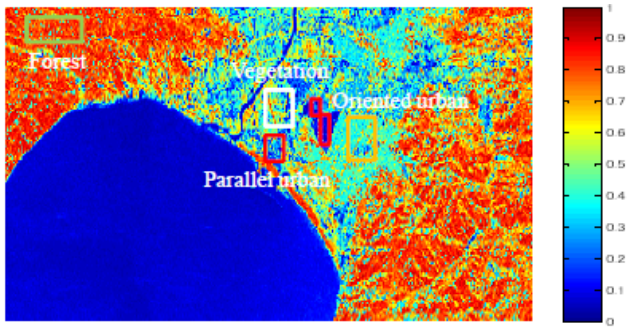

(a) Estimated results by using (12) (Winter Season)

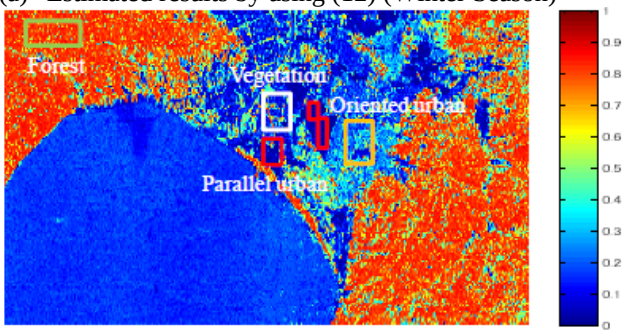

(b) Estimated results by using (15) (Winter Season)

Fig.18 Vegetation/Forest/Urban discrimination by using each index (Winter season data).

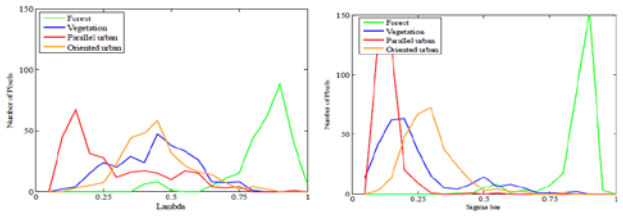

Fig.19 Histograms of selected areas in Fig.18.

6. DECOMPOSITION FOR POLARIMETRIC SAR INTERFEROMETRY

This research was intended to extend the model-based decomposition techniques to POL-InSAR data. In the POLSAR analysis of covariance matrix, we only have 4 independent observables with reflection symmetry targets. However the models discussed in Sect.2 have 5 or more unknowns. Their techniques handle this uncertainty with some assumptions.

Single and double bounce components are important when we estimate soil moisture of the vegetated area. Covariance matrix of the each component has one unknown. In the Freeman and Yamaguchi method, one of them is determined by 1 or -1 depending on the dominant component. On the other hand, Arii method uses the assumption that dot product of them becomes -1. They are semi-empirical assumptions.

When we extend the decomposition to the POL-InSAR data, we can acquire 4 additional independent observables. Three complex coherences corresponding to each component are the newly added unknowns. Therefore, there are one-freedom for estimating the unknowns in single or double-bounce component. This is the main concept in this approach. This concept was almost well demonstrated highly coherent POL-InSAR datasets, i.e. E-SAR data, SIR-C/X-SAR. However, the method was not work properly for the ALOS/PALSAR data. Main reason for this will be rack of coherence due to temporal decorrelation. However, POL-InSAR approach for the decomposition is still an attractive problem and has a potential to extract furthermore information from the data. Therefore, we have been struggling to find a new processing technique for improvement.

7. CONCLUSION

In this project, we evaluate various model-based polarimetric decomposition techniques. To enrich and improve the decomposition accuracy, we have also proposed to apply polarization-basis rotation before the decomposition. In this project we have clarify that 1) the modified volume scattering model proposed by Dr. Arii and van Zyl is acceptably accurate in comparison with that of conventional ones, 2) the polarization-basis rotation improves mis-classification between forest/vegetation and oriented urban, 3) the modified volume scattering model is stable and robust for the polarization-basis rotation of the covariance matrix. We also intended to extend the method to the POL-InSAR data. However available results could not be obtained at this stage due to lack of coherence. This is one of the further studies to be done in near future.

8. REFERENCES

[1] S. R. Cloude and E. Pottier, “A review of target decomposition theorems in radar polarimetry,” IEEE Trans. Geoscience and Remote Sens., vol. 34, no. 2, pp. 498–518, Mar. 1996.

[2] A. Freeman and S. L. Durden, “A three-component scattering model for Polarimetric SAR data,” IEEE Trans. Geoscience and Remote Sensing, vol.36, no.3, pp.963-973, May 1998.

[3] Y. Yamaguchi, T. Moriyama, M. Ishido, and H. Yamada, “Four-component scattering model for polarimetric SAR image decomposition,” IEEE Trans. Geosci. Remote Sensing, vol.43, no.8, pp.1699–1706, Aug. 2005.

[4] Y. Yajima, Y. Yamaguchi, R. Sato, H. Yamada, and W. -M. Boerner, “Polsar image analysis of wetlands using a modified four-component scattering power

decomposition," IEEE Trans. Geoscience and Remote Sens., vol. 46, no. 6, pp. 1667–1773, June 2008.
[5] M. Arii, Retrieval of Soil moisture under Vegetation using Polarimetric RADAR, Ph.D dissertion, California Institute of Technology, Pasadena, California, 2009.
[6] M. Arii, J. J. van Zyl, and Y. Kim "Adaptive decomposition of polarimetric SAR covariance matrix," IGARSS 2009, Cape Town, South Africa, July. 2009.
[7] M. Arii, J. J. van Zyl, and Y. Kim, "A general characterization for polarimetric scattering from vegetation canopies," IEEE Trans. Geosci. Remote Sens., vol. 48, no. 9, pp.3349-3357, Sept. 2010.
[8] Y. Yamaguchi, A. Sato, W. M. Boerner, R. Sato, and H. Yamada, "Four-component scattering power decomposition with rotation of coherency matrix," to appear in IEEE Trans. Geosci. Remote Sens.
[9] H.Yamada, Y.Yamaguchi, Y.Kim, E.Rodriguez, and W.M.Boerner, "Polarimetric SAR interferometry for forest analysis based on the ESPRIT algorithm," IEICE Trans. Electron., vol.E84-C, no.12, pp.1917-1924, Dec.2001.
[10] H.Yamada, Y.Yamaguchi, W.M.Boerner, "Forest Height feature extraction in polarimetric SAR interferometry by using rotational invariance property," Proc. of IGARSS 2003, July 2003.
[11] H.Yamada, H.Okada, Y.Yamaguchi, "Accuracy Improvement of ESPRIT-based Polarimetric SAR Interferometry for Forest Height Estimation," Proc. of IGARSS 2005, July 2005.
[12] H.Yamada, M.Yamazaki, and Y.Yamaguchi, "On scattering model decomposition of POLSAR image and its application to the ESPRIT-Base Pol-InSAR," Proc. EUSAR 2006, May 2006.
[13] H. Yamada, Y. Yamaguchi and R. Sato, "Polarimetric scattering model decomposition for POL-InSAR data," Proc. of IGARSS 2008, July 2008.
[14] H. Yamada, Y. Yamaguchi and R. Sato, "Scattering component decomposition for POL-InSAR data and its application," Proc. of IGARSS 2009, July 2009.
[15] J. J. van Zyl, "Application of Clouds's target decomposition theorem to Polarimetric imaging radar data," Radar Polarimetry, vol.SPIE-1748, pp.184-212, 1992.
[16] Y. Kim and J. J. van Zyl, "Comparison of forest estimation techniques using SAR data," Proc. IGARSS2001, Sydney, Australia, July 2001.